Fu *et al.*
Chinese Journal of Mechanical Engineering (2023) 36:153
https://doi.org/10.1186/s10033-023-00974-7

Chinese Journal of Mechanical Engineering

ORIGINAL ARTICLE

Open Access

Design of A Novel Wheel-Legged Robot with Rim Shape Changeable Wheels

Ze Fu[1], Hao Xu[1], Yinghui Li[1] and Weizhong Guo[1*]

Abstract

The wheel-legged hybrid structure has been utilized by ground mobile platforms in recent years to achieve good mobility on both flat surfaces and rough terrain. However, most of the wheel-legged robots only have one-directional obstacle-crossing ability. During the motion, most of the wheel-legged robots' centroid fluctuates violently, which damages the stability of the load. What's more, many designs of the obstacle-crossing part and transformation-driving part of this structure are highly coupled, which limits its optimal performance in both aspects. This paper presents a novel wheel-legged robot with a rim-shaped changeable wheel, which has a bi-directional and smooth obstacle-crossing ability. Based on the kinematic model, the geometric parameters of the wheel structure and the design variables of the driving four-bar mechanism are optimized separately. The kinetostatics model of the mobile platform when climbing stairs is established to determine the body length and angular velocity of the driving wheels. A prototype is made according to the optimal parameters. Experiments show that the prototype installed with the novel transformable wheels can overcome steps with a height of 1.52 times of its wheel radius with less fluctuation of its centroid and performs good locomotion capabilities in different environments.

Keywords Mobile platform, Transformable wheel-legged robot, Kinematics analysis, Mechanical design, Obstacle crossing

1 Introduction

Mobile platforms determine the motion performance of robots. Especially in the fields of military reconnaissance, disaster rescue and extra-terrestrial exploration, the obstacle-crossing ability is highly demanded. At present, ground mobile platforms can be divided into wheel type, leg type and crawler type according to their motion mode.

Among them, wheel-based locomotion is the simplest and most efficient [1]. Therefore, wheeled robots are widely used in the design of road-carrying robots (such as unmanned intelligent vehicles) [2, 3] and indoor robots [4, 5]. However, if the wheeled robot encounters an obstacle with a height greater than the radius of its wheel, it will not be able to pass it [6]. Therefore, the application in the complex terrain of the wheeled robot is limited by its poor obstacle-crossing ability. With the help of bionic walking gaits, the legged robot has good motion performance on uneven surfaces [7, 8]. However, due to the complexity of the control strategy of the leg mechanism [9] and the need for terrain prediction and collection information [10], their moving speed is much slower than that of the wheeled robots. At the same time, the fluctuation of the centroid and the collision between the foot and the ground [11] lead to low energy utilization efficiency.

The wheel-legged hybrid robot is another important research direction. The early wheel-legged hybrid structure is fixed. WHEGS's [12] rimless wheel has three spokes with hooks at the end of them. It mimics the barbs on the insects' legs and overcomes rocks by hooking on their edges. Rhex [13] adopts the half-circular rim as

*Correspondence:
Weizhong Guo
wzguo@sjtu.edu.cn
[1] State Key Laboratory of Mechanical System and Vibration, Shanghai Jiao Tong University, Shanghai 200240, China

legs to expand the motion range. RoMiRAMT [14] uses rotating wheels with six legs and adds a spine to lift or lower the body, which allows the robot to climb higher obstacles. This kind of wheel-legged hybrid robot with a fixed structure sacrifices the ability to move quickly on flat ground in exchange for the ability to cross complex terrain. At the same time, some scholars have proposed another design idea of wheel-legged robot, which attaches a round wheel to the end of the leg. For example, Alduro [15], PAW [16], Hylos [17], Shrim and others have adopted this design method, which enables the robot to move on flat ground smoothly with round wheels, and to pass through obstacles on unstructured terrain with the help of the characteristics of discrete landing points of the leg mechanisms. But since both the legs and wheels of this kind of robot have degrees of freedom, the number of driving motors needs to be increased. This will lead to the complexity of its control strategy and possible damage on harsh terrain.

Over the past few years, in order to make the robot transform between the wheel mode and leg mode so as to combine the advantages of both types [18, 19], many scientists have studied transformable wheel-legged mobile platforms. The surface of Impass's [20] wheel is full of holes. The gear mechanism drives the rack on the spoke in the hole so that the spoke can extend out of the hole. Furthermore, the structure can switch between the round wheel and the spoke wheel. Quattroped's [21] wheel can be separated into two semicircular legs with obstacle-crossing capability. Lee [22] Proposed a transformable wheel based on composite membrane origami which can bear more than 10 kN load. The proposed design rule and thick membrane are suitable for high-payload applications. QuadRunner [23] is a novel transformable quasi-wheel-legged robot that combines quadruped and wheel locomotion using a semicircular leg-wheel design with a Trotting Wheel gait. WheeLeR [24] uses the center gear to open or close the wheel rim. When opened, the rim can hook the edge of the obstacle and lift the robot to cross the obstacle. FUHAR [25] uses a four-bar linkage to drive the circular wheel rim into six claws. Dynamic and simulation models are established to verify its obstacle-crossing performance. Ryu et al. [26] proposes a shape-morphing wheel for high-speed step climbing in mobile robots, extending wheel shape to overcome obstacles using centrifugal force.

Most of these wheel-legged hybrid robots adopt structure similar to a claw to hook the edge of obstacles and cross over them, which lead to violent fluctuations of the mobile platform's centroid and damage the stability of the load. At the same time, due to the asymmetry of the mechanism, most of the wheel-legged structures only have one-directional obstacle-crossing ability, which limits their application in complex terrain. Moreover, the geometrical parameters of the wheel determine its obstacle-crossing ability and the design variables of the driving mechanism determine the difficulty of transformation. But these two design parts are highly coupled generally, which limits the optimal performance in both aspects.

In this paper, a novel wheel-legged robot with rim shape changeable (RSC) wheels is designed, which has the ability of bi-directional obstacle-crossing. During the climbing process, the rim contacts the obstacle's surface smoothly to reduce the centroid fluctuation of the mobile platform. Different from the previous design in which the geometric shape of the wheel is highly coupled with mechanism configuration, the kinematic model of the RSC wheel is first established, and the relationship between its geometric parameters and climbing ability is revealed. On this basis, the optimal geometric parameters of the wheel meeting the obstacle-crossing requirements are selected, and then the design variables of the driving four-bar mechanism are optimized to improve the transformation efficiency. The kinetostatics model of the mobile platform when climbing stairs is established to determine the body length and angular velocity of the driving wheels. Experiments show that the prototype is able to traverse rough terrain steadily.

The organization of this paper is as follows: Section 2 presents the kinematic model of the RSC wheel when crossing obstacles. The optimal design parameters of the driving four-bar mechanism are formulated in Section 3. Kinetostatics of the whole wheel-legged mobile platform is modeled to select the robot platform parameters in Section 4. Section 5 conducts the prototype experiment to verify the obstacle-crossing stability and terrain adaptability of the robot, and Section 6 has concluding remarks.

2 Kinematic Model of the Transformable Wheel in Obstacle Crossing Process

The wheel with the shape changeable rim is essentially an equally divided circle, and the arc after equal division rotates around a point on it. As shown in Figure 1, take the wheel rim divided into three parts as an example to model the kinematics of the climbing process. The structure of the RSC wheel is determined by r, n, θ and δ, which correspond to the wheel radius, the number of equally divided arcs, the rotation angle of each arc, and the central angle of each arc between their endpoint and the rotation point respectively.

The RSC wheel rotates periodically on the flat surface, and each period includes two stages: the arc rolling stage and tip rotating stage. As shown in Figure 2(a), the former stage is the rotation of the circle in which arc $\widehat{BC}$ in

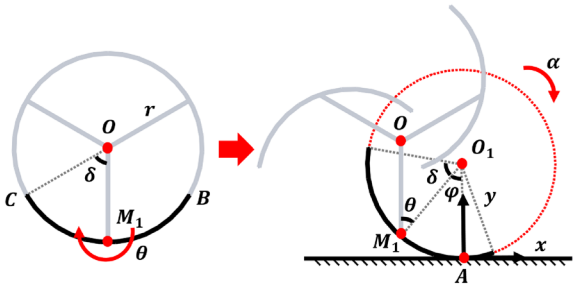

Figure 1 The RSC wheel and its motion coordinate system

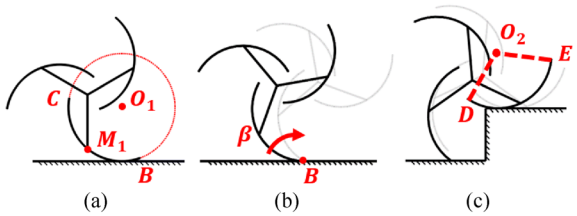

Figure 2 Movement process of the RSC wheel. Stage of (**a**) Arc rolling, (**b**) Tip rotating, (**c**) Contacting the obstacle surface

contact with the ground is located, and the trajectory of any point on the RSC wheel is the cycloid.

Assuming that at the beginning, the contact point between $\widehat{BC}$ and the ground is A, and $\overline{OM_1}$ is vertical. The center angle of the arc rotation point M_1 and contact point A is φ. Take A as the origin and establish the coordinate system. The rotation angle of circle O_1 is α, and the trace of O_1 is

$$\begin{cases} O_{1x} = r\alpha, \\ O_{1y} = r. \end{cases} \tag{1}$$

And the trace of M_1 is cycloid, which has the initial phase angle φ. The trace of M_1 can be written as

$$\begin{cases} M_{1x} = r((\alpha+\varphi) - \sin(\alpha+\varphi)) + r\varphi, \\ M_{1y} = r(1-\cos(\alpha+\varphi)). \end{cases} \tag{2}$$

By rotating O_1M_1 counterclockwise around M_1 at the transform angle θ, the trace of the wheel center $\boldsymbol{O}$ in the first stage can be written as

$$\begin{bmatrix} O_x \\ O_y \end{bmatrix} = \begin{bmatrix} M_{1x} \\ M_{1y} \end{bmatrix} + \boldsymbol{R}_1 \begin{bmatrix} O_{1x} - M_{1x} \\ O_{1y} - M_{1y} \end{bmatrix}, \tag{3}$$

where $\boldsymbol{R}_1$ is the rotation matrix:

$$\boldsymbol{R}_1 = \begin{bmatrix} \cos\theta & -\sin\theta \\ \sin\theta & \cos\theta \end{bmatrix}. \tag{4}$$

As shown in Figure 2(b), when the rotation angle is:

$$\alpha = 360^\circ / n - \delta - \varphi, \tag{5}$$

where $\delta \le 180^\circ / n$, the arc $\widehat{BC}$'s endpoint B contacts the ground, and the wheel enters the tip rotating stage. At this time, all the points on the wheel rotate the angle of β around B. The trace of O_1 and M_1 can be expressed as

$$\begin{bmatrix} M_{1x} \\ M_{1y} \end{bmatrix} = \begin{bmatrix} B_x \\ B_y \end{bmatrix} + \boldsymbol{R}_2 \begin{bmatrix} M_{1x} - B_x \\ M_{1y} - B_y \end{bmatrix}, \tag{6}$$

$$\begin{bmatrix} O_{1x} \\ O_{1y} \end{bmatrix} = \begin{bmatrix} B_x \\ B_y \end{bmatrix} + \boldsymbol{R}_2 \begin{bmatrix} O_{1x} - B_x \\ O_{1y} - B_y \end{bmatrix}, \tag{7}$$

where $\boldsymbol{R}_2$ is the rotation matrix:

$$\boldsymbol{R}_2 = \begin{bmatrix} \cos\beta & \sin\beta \\ -\sin\beta & \cos\beta \end{bmatrix}. \tag{8}$$

Similarly, the trace of the wheel center O at this stage can be obtained from Eq. (3). This paper evaluates the obstacle-crossing ability by taking climbing stairs as an example. As shown in Figure 2(c), the height of the step is H, the arc $\widehat{DE}$ will touch the step surface before contacting the ground. When $\widehat{DE}$ is tangent to the step surface, the following condition is satisfied:

$$O_{2y} - r - H = 0. \tag{9}$$

Thus, the height of the step that can be climbed is:

$$H = O_{2y} - r. \tag{10}$$

If the number of equally divided arcs is n, the center angle of each arc is $360^\circ/n$. That is, the angle between $\overline{OO_1}$ and $\overline{OO_2}$ is $360^\circ/n$. The coordinate of O_2 in Eq. (10) can be described as

$$\begin{bmatrix} O_{2x} \\ O_{2y} \end{bmatrix} = \begin{bmatrix} O_x \\ O_y \end{bmatrix} + \boldsymbol{R}_3 \begin{bmatrix} O_{1x} - O_x \\ O_{1y} - O_y \end{bmatrix}, \tag{11}$$

where $\boldsymbol{R}_3$ is the rotation matrix:

$$\boldsymbol{R}_3 = \begin{bmatrix} \cos(\frac{2\pi}{n}) & -\sin(\frac{2\pi}{n}) \\ \sin(\frac{2\pi}{n}) & \cos(\frac{2\pi}{n}) \end{bmatrix}. \tag{12}$$

By adopting the above obstacle climbing method, the rim can smoothly and rapidly move on the step's surface once it contacts the step. When $H = 15$ cm, $r = 10$ cm, $n = 3$, $\delta = 60^\circ$ and $\theta = 50^\circ$, the trace of the wheel center O during the process of climbing steps can be derived by combining Eqs. (3) and (10), which is shown in Figure 3.

The RSC wheel experiences the arc rolling stage on the ground and the rotation stage around the end of the arc (P_1 to P_2) - contacting the step (at P_2) - the arc rolling

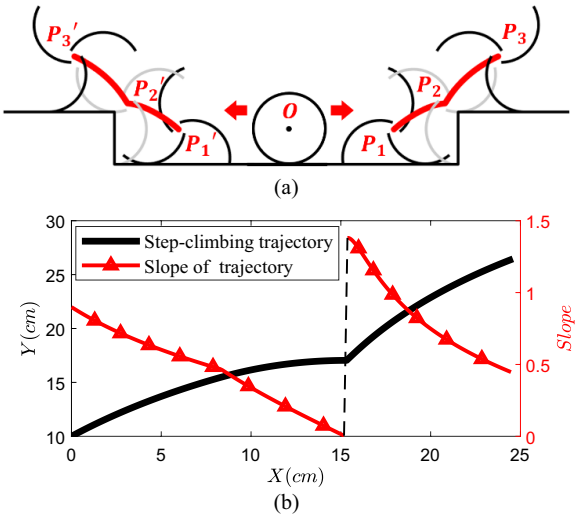

Figure 3 Obstacle climbing process when $H = 15$ cm, $r = 10$ cm, $n = 3, \delta = 60°$ and $\theta = 50°$: (**a**) Bi-direction trajectory of the wheel center O, (**b**) The change of trajectory slope

stage on the step (P_2 to P_3) as shown in Figure 3(a). At the beginning (at P_1) and the end (at P_3) of this process, the height of the wheel center O is consistent with the height of the center of the round wheel on the ground and the step, that is, 10 cm and 25 cm respectively. With the completion of climbing, the RSC wheel moves 24.6 cm in the horizontal direction. The motion range of the centroid is between 10cm and 25 cm during the whole process.

Figure 3(b) shows the change of the trajectory slope. Except at P_2, the slope changes continuously, and the maximum value does not exceed 1.5. The slope change at P_2 is 1.45, and it is always positive throughout the process. The centroid of the wheel fluctuates mildly in the whole process, and the motion stability is good.

3 Design of Transformable Wheel Mechanism

Based on the kinematic model mentioned in Section 2, this paper proposes a method for the separation design of the obstacle-crossing structure and the driving mechanism.

The wheel structure is designed first to promote the obstacle-crossing ability and the driving mechanism is designed later to make the transformation process easier. The schematic diagram of our proposed design framework is illustrated in Figure 4.

3.1 Concept of the Wheel Mechanism

The obstacle-crossing capability can be indicated by the ratio of the maximum height of the obstacle the wheel can overcome H_m to the wheel radius in round shape r [27], and it depends on the geometric parameters of the RSC wheel. The mathematical expression of H_m/r is

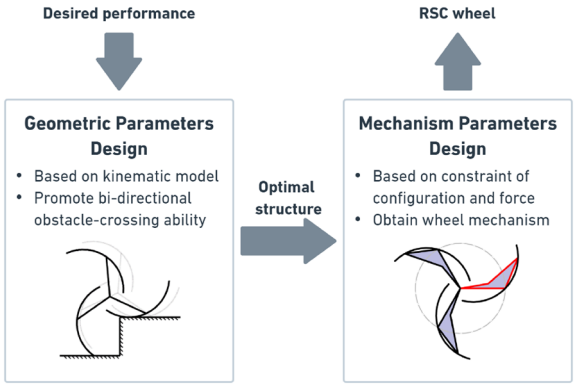

Figure 4 Schematic diagram of the proposed two-stage design framework of transformable wheel mechanism

analyzed by taking the RSC wheel which has four divided legs as an example. As shown in Figure 5, when overcoming the obstacle with maximum height, the arc's endpoint B should be at the intersection of the ground and the vertical surface of the step.

The geometric constraint in this position is:

$$B_x = O_{2x}. \tag{13}$$

Considering reducing the structure complexity, the number of arcs in RSC wheel is set to be no more than 6. Due to the symmetry of the structure, both the rotation angle of each arc θ and the central angle of each arc between their endpoint and the rotation point δ vary from 0° to 90°. Based on these range limits, the relationship between H_m/r and n, δ, θ can be derived by substituting Eq. (13) into the kinematic model in Section 2, which is shown in Figure 6.

Figure 6 illustrates that regardless of the number of equally divided legs n, H_m/r increases with θ and δ. As mentioned above, the maximum value of δ is $180°/n$. In this case, δ is half of the central angle corresponding to each arc and the configuration of the wheel is symmetrical. Thus, δ is determined as $180°/n$ to obtain bi-directional barrier-overcoming capacity. From Figure 6, the relationship between n, θ and H_m/r can be derived in Figure 7.

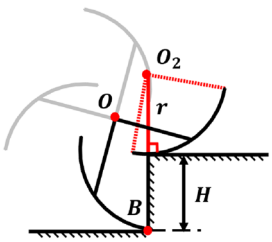

Figure 5 The position of the RSC wheel with four legs when overcoming the obstacle with maximum height

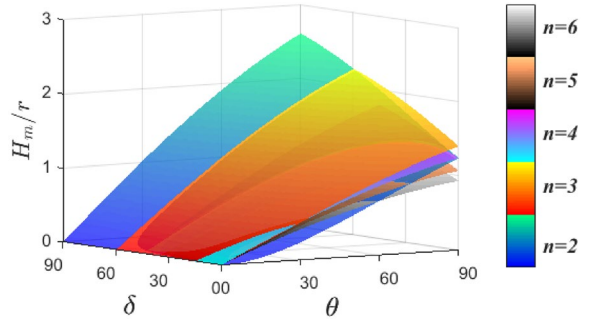

Figure 6 Relationship between n, θ, δ and the obstacle crossing ability H_m/r

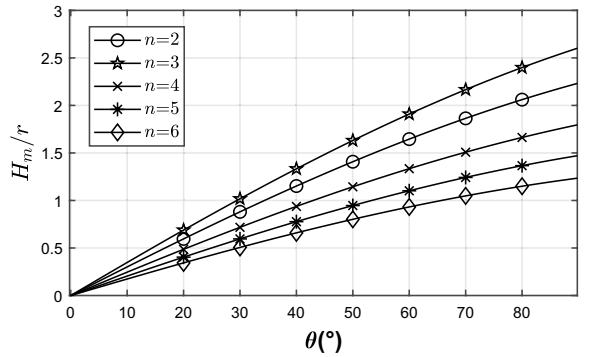

Figure 7 Relationship between n, θ and the obstacle-crossing ability H_m/r when $\delta = 180°/n$

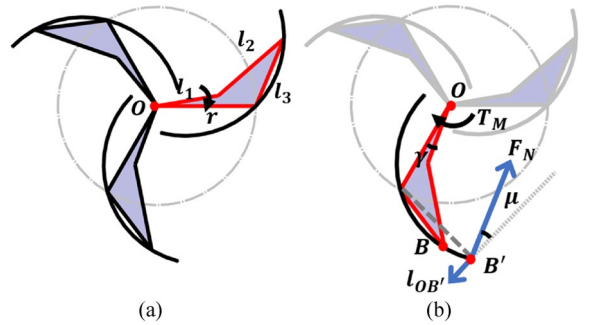

Figure 8 The RSC wheel driven by the four-bar mechanism: (**a**) Schematic diagram of the mechanism, (**b**) Free body diagram of the wheel during the transformation process

Figure 7 illustrates that under the same θ, the obstacle-crossing performance is strongest when $n = 3$, slightly weaker when $n = 2$, and gets worse when $n > 3$ as n increases. Therefore, the structure with three legs after transformation is chosen as shown in Figure 8.

As shown in Figure 8(a), based on the optimal structure, the transformation driving part will be designed in the following. For compactness and reliability, three planar four-bar mechanisms are used to drive the transformation of the wheel, in which the rocker l_1 provides the driving force.

3.2 Selection of Design Variables Based on Kinematics

The design variables, especially the length of linkage l_1, l_2, l_3, are analyzed and properly selected based on the kinematic model in this part. Figure 6 reveals that the larger the transformation angle θ, the stronger the barrier-crossing capability. Therefore, an optimization problem with the maximum θ as the objective can be constructed.

Considering the clockwise transformation of the rim, the relationship between θ_m and the length of each linkage is:

$$\theta_m = \arccos \frac{l_3^2 + r^2 - (l_1 + l_2)^2}{2 l_3 r} + \arcsin \frac{l_3}{2r} - 90°. \tag{14}$$

The next step is to perform the dimensional synthesis of the mechanism. The lengths of the three links need to satisfy some constraints. The condition for the existence of the four-bar mechanism is:

$$\begin{cases} l_1 + l_2 + l_3 > r, \\ r + l_2 + l_3 > l_1, \\ l_1 + r + l_3 > l_2, \\ l_1 + l_2 + r > l_3. \end{cases} \tag{15}$$

The dimension parameters of the linkages are also limited by the size of the structure to avoid motion interference:

$$\begin{cases} r < l_1 + l_2 < r + l_3, \\ l_3 < 2r \sin \dfrac{\delta}{2}, \\ l_1 + r > l_2 + l_3. \end{cases} \tag{16}$$

Besides, the torque required for transformation should be small to ensure the successful shape change of the rim. After the gear reduction, there is maximum torque $T_M \leq 3\ \mathrm{N} \cdot \mathrm{m}$. As shown in Figure 7(b), by the principle of virtual work, the following equation can be obtained:

$$T_m \mathrm{d}\gamma = F_N \cos \mu \mathrm{d}B'. \tag{17}$$

By combining Eqs. (14) to (17), the optimization variable space can be drawn as Figure 9.

In Figure 9, the red dot indicates the optimal four-bar mechanism parameters satisfying the constraints within the variable space, which are:

$l_1 = 0.625\, r, l_2 = 0.880\, r, l_3 = 0.735\, r.$

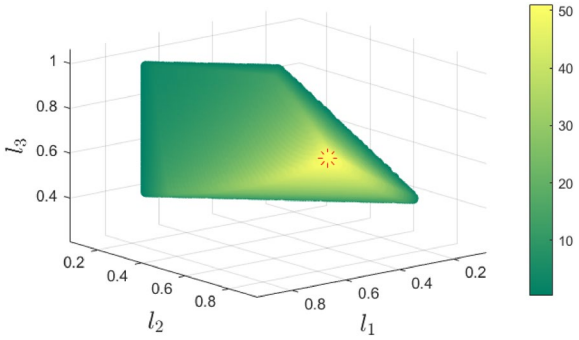

Figure 9 Relationship between the θ_m and the length of linkages under the constraints. The red dot indicates the location of the optimal parameters

The maximum height of the step is set as 15 cm. From Figure 7, the corresponding minimum radius of the wheel $r_{min} = 9.09$ cm. Taking the machining error and the stability margin into account, r is designed as 10 cm. Thus, the optimized design variables are

$l_1 = 6.25$ cm, $l_2 = 8.80$ cm, $l_3 = 7.35$ cm.

The mechanism with optimized design variables is shown in Figure 10. The Maximum clockwise transformation angle θ_m reaches 50.4 ° and H_m/r reaches 1.52. Each leg is connected to the center turning disk so that the whole transformation can be driven by just one motor. Active bar l_1 rotates clockwise or counterclockwise to change the wheel into forward or backward direction motion mode respectively, thus providing the mobile platform with a bi-directional obstacle-crossing capability.

4 Design of Mobile Platform

To design the mobile platform equipped with the RSC wheel, there are other parameters that need to be determined, such as the body length. In addition, in order to select the type of driving motor, it is necessary to estimate the rotation speed of the RSC wheel. The optimization of these parameters will be carried out based on a kinetostatics model.

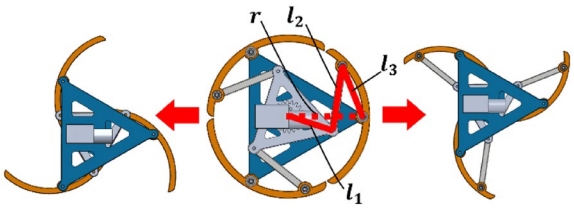

Figure 10 The wheel mechanism with optimum design variables

4.1 Kinetostatics Analysis of the Mobile Platform

The free body diagram (FBD) of the mobile platform installed with the RSC wheel is shown in Figure 11. The robot consists of three parts: the RSC wheel, the body and the passive assistant wheel. Only the former two parts are analyzed, which ignores the influence of the structure of the passive assistant wheel. Considering the symmetry of the structure, the FBD of the RSC wheel and body is planar.

Since the transformation driving motor and the motion driving motor are arranged on the axis of the RSC wheel and the mass of the body is quite small compared to the mass of the RSC wheel, it is assumed that the mass of the robot is approximately concentrated in the RSC wheel center. The wheel rotation can be regarded as quasi-statically [28] due to its slow and constant speed. Also, the friction force on the passive assistant wheel is ignored, so there is only vertical support force F_y applied to the body. Based on the above assumptions, the kinetostatics analysis of the wheel and the body can be carried out. Table 1 explains the parameters of the kinetostatics model.

The success of the step-climbing depends largely on F_N and f. The greater F_N, the more stable the mobile platform will be. And large f ensures that the robot will not slip during this process. Since this process is relatively gentle, based on the D'Alembert principle, the kinetostatics equations of the robot on point O can be obtained to optimize the design variables:

$$\begin{cases} f = -M\omega^2 r\cos\varphi, \\ F_y + F_N - Mg = -M\omega^2 r\sin\varphi, \\ fr\sin\varphi - F_N r\cos\varphi + F_y\sqrt{L^2 - (H + R\sin\varphi)^2} = 0. \end{cases} \tag{18}$$

The expression of support force on the active wheel at P can be written by revising Eq. (18) as

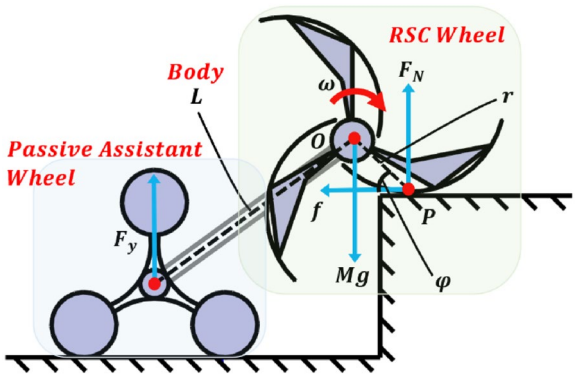

Figure 11 The free body diagram of the mobile platform during the obstacle-crossing process

Table 1 Parameters of the kinetostatics model

Parameter	Description	Value
M	Mass of the robot	5.2 kg
r	RSC wheel radius (Wheel mode)	0.1 m
ω	Angular velocity of the RSC wheel	
φ	Angle between $\overline{OP}$ and step surface (P is the contact point between the arc and the step)	
g	Acceleration of gravity	9.8 kg/m^2
F_N	Support force on the active wheel at P	
F_y	Support force on the body	
f	Frictional force on the active wheel at P	
H	Height of the step	1.5 m
L	Body length	

$$F_N = \frac{M\left(g - r\omega^2 \sin\varphi - \frac{r^2\omega^2 \sin\varphi \cos\varphi}{\sqrt{L^2-(H+r\sin\varphi)^2}}\right)}{1 + \frac{r\cos\varphi}{\sqrt{L^2-(H+r\sin\varphi)^2}}}. \quad (19)$$

Equation (19) can be used to study the influence of body length L and the angular velocity of the drive motor ω on the obstacle-crossing performance. The mass of the robot M and the RSC wheel radius r (in wheel mode) is constant. According to the kinematic model in Section 2, in the extreme case, the initial angle between $\overline{OP}$ and the step surface is 50°. And when the robot is on the step, $\overline{OP}$ is vertical to the step surface. Thus, φ varies from 50° to 90° during the step-climbing process. The relationships between F_N and L, φ (when $\omega = 1$ rad/s) and the relationships between F_N and ω, φ (when $L = 0.3$ m) are shown in Figure 12.

Figure 12(a) illustrates that the increase in body length contributes to the stability of the robot during the obstacle-overcoming process. The reason is that if the passive assistant wheel is away from the centroid of the robot, the possibility of body overturning can be reduced. At the same time, a long platform provides more space to carry the load. Figure 12(b) illustrates that when the motor power is a certain value, the angular velocity should be as small as possible. Considering the overall size limitations, L is designed as 0.35 m and ω is chosen as 1 rad/s.

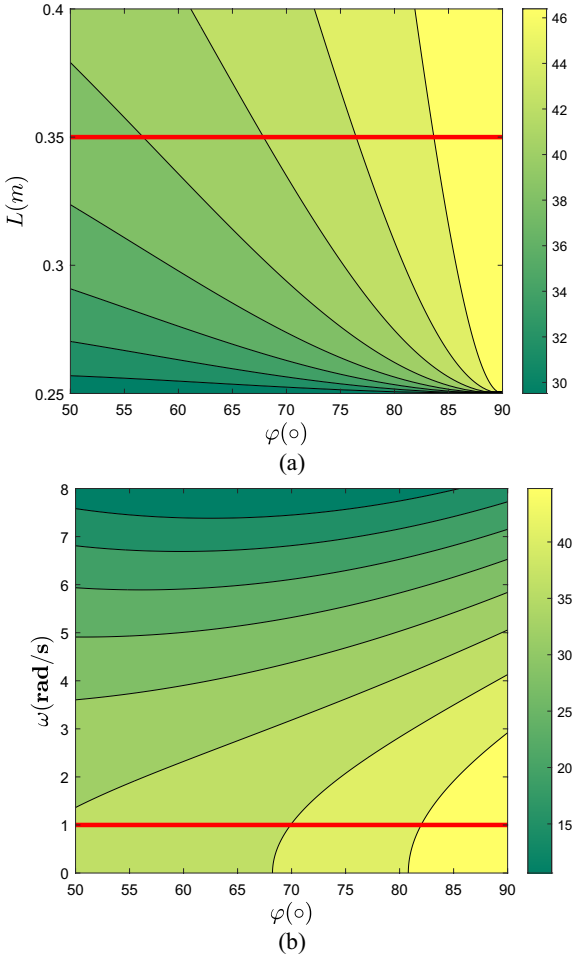

Figure 12 Influence of L and ω on the obstacle-climbing performance of the mobile platform: (**a**) Relationship between F_N and L, φ when $\omega = 1$ rad/s (Red line represents that L is finally chosen as 0.35 m), (**b**) Relationship between F_N and ω, φ when $L = 0.3$ m (Red line represents that ω is finally chosen as 1 rad/s)

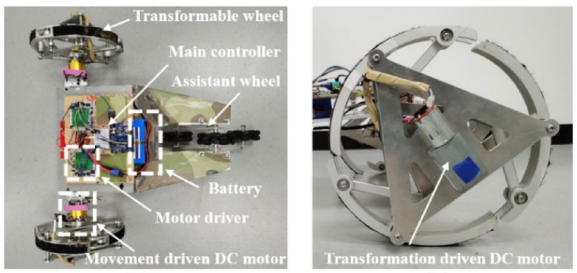

Figure 13 Prototype of the wheel-legged robot: (**a**) Top view of the prototype, (**b**) Side view of the RSC wheel

4.2 Prototype Design

Based on the previous design, the prototype with two RSC wheels is developed as shown in Figure 13. The overall size of the prototype is 46 × 40 × 24 cm^3. The rotation of the wheel is driven by DC encoder motors, with the model CHR-42GP-775 and a reduction ratio of 1:92. The transformation of the RSC wheel is driven by brushless DC motors. The model of the motor is CHW-GW4632-370 and the reduction ratio of 1:32.

The control system of the robot consists of a main controller and two motor drivers. The model of the main controller is Arduino UNO, and the two motor drivers

are both dual H-bridge 60A motor drive modules, which control the motion drive motor and the transformation drive motor respectively. The whole system is powered by a lithium battery with a capacity of 9800 mhA, which provides 12 V voltage to the controller and the motor drivers. It can ensure one-hour continuous operation for the robot. The specific parameters of the prototype are listed in Table 2.

Before the experiments, in order to verify whether the maximum transformation angle of the RSC wheel can reach 50°, a sensitivity analysis of the obstacle-crossing capability to the dimensions of the transformation driving mechanism was carried out to exclude the effect of machining errors on the performance of the prototype. Take partial derivatives on both sides of Eq. (14):

$$\frac{\partial \theta_m}{\partial l} = \left[\frac{\partial \theta_m}{\partial l_1} \ \frac{\partial \theta_m}{\partial l_2} \ \frac{\partial \theta_m}{\partial l_3} \right]^{\mathrm{T}}. \tag{20}$$

Equation (20) can be used to analyze the relationship between the change of the obstacle-crossing ability and the change of the length of three transformation driving links. When one of the lengths of the linkage l_1, l_2, l_3 changes by ten thousandths (m) and the other two remain unchanged, while the three parameters still satisfy the constraint relations of Eqs. (15) to (17), Figure 14 can be obtained. In Figure 14, the red dots indicate the most sensitive location to the change of design parameters.

In Figure 14, the red dots indicate the most sensitive location to the change of design parameters. It can be obtained that under the currently designed parameters, θ_m can be affected by the length of the linkages to the maximum extent as:

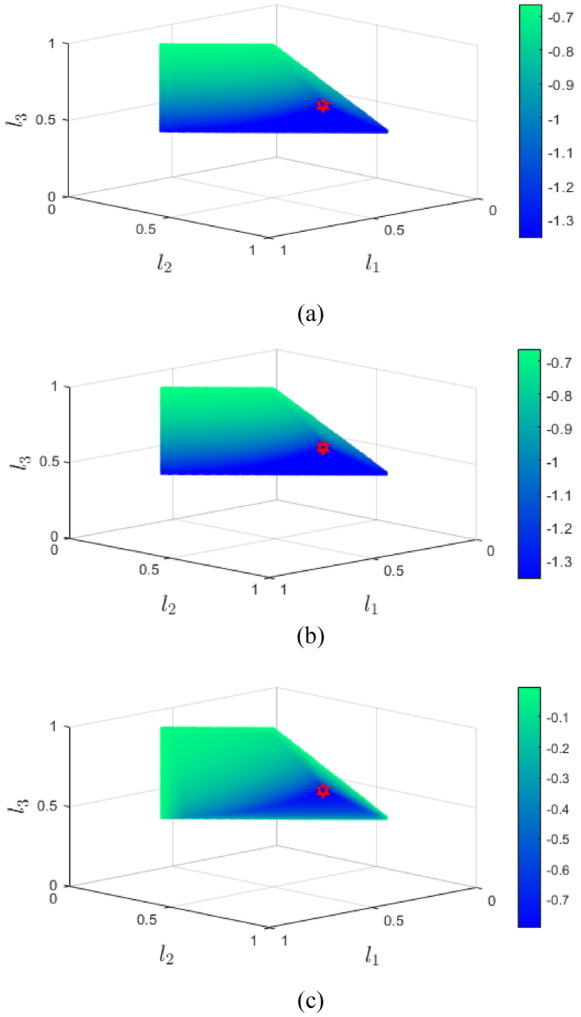

Figure 14 Sensitivity of RSC wheel's transformation angle $\Delta\theta_m$ to driving mechanism's linkage lengths: (**a**) l_1 changes 0.0001 m, while l_2, l_3 remain unchanged, (**b**) l_2 changes 0.0001 m, while l_1, l_3 remain unchanged, (**c**) l_3 changes 0.0001 m, while l_1, l_2 remain unchanged

Table 2 Parameters of the robot prototype

Items	Features
Total mass	5.2 kg
RSC wheel radius	0.1 m
Assistant wheel equivalent radius	0.13 m
Body length	0.35 m
Battery	Lithium battery (9800 mhA,12 V)
Body materials	Aluminum alloy
Maximum transformation angle of the RSC wheel	50.2°
Maximum speed	1.67 m/s (Wheel mode)
Transformation drive motor	Rated torque: 1.5 N·m
	Rated speed: 7 r/min
Motion drive motor	Rated torque: 6 N·m
	Rated speed: 80 r/min

$$\left(\frac{\partial \theta_m}{\partial l}\right)_{\max} = \left[1.3 \ 1.3 \ 0.7 \right]^{\mathrm{T}} (^\circ/\mathrm{mm}). \tag{21}$$

Then, according to the relationship between the transformation angle and the maximum height that the RSC wheel can cross shown in Figure 7, we can obtain:

$$\left(\frac{\partial H_m}{\partial l}\right)_{\max} = [4.4 \ 4.4 \ 2.4]^{\mathrm{T}}. \tag{22}$$

Equation (22) shows that every 1 mm machining error of the three linkages l_1, l_2, l_3 will reduce the maximum obstacle-crossing height by 4.4 mm, 4.4 mm and 2.4 mm, respectively. The material of the linkages in the prototype is aluminum alloy and its machining

accuracy is 0.02 mm, so the effect on the obstacle-crossing height is basically negligible. By measurement, the maximum transformation angle of the RSC wheel in the prototype is actually 50.2°.

5 Experiments

To verify the obstacle-crossing ability and stability of the prototype and test whether the kinematics and kinetostatics model established above are correct, the experiments are carried out in the real environment shown in Figure 15. The surface of the RSC wheel is pasted with a common tire material to increase the friction between it and the ground. The prototype was free from human interference throughout the obstacle-crossing process.

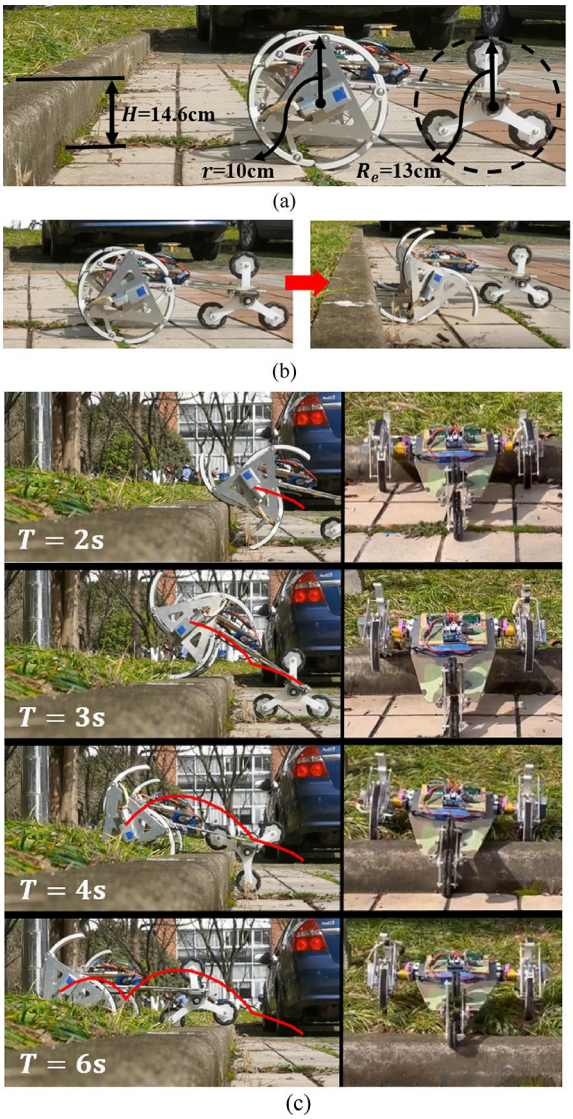

Figure 15 Obstacle-crossing experiment of the prototype: (**a**) Environment of the experiment, (**b**) Robot switches motion modes in front of the step, (**c**) Step-climbing process

In Figure 15(a), the robot is in wheel mode, and its speed can reach a maximum of 1.67 m/s (3.63 robot lengths per second), which can meet the efficient locomotion requirement on flat ground. The height of the step in front of the robot is 14.6 cm, and the ratio of the step height to the radius of the RSC wheel H/r is 1.46. The equivalent radius of the passive assistant wheel is 13 cm.

In Figure 15(b), when encountering an obstacle, the robot will switch from wheel mode to leg mode, in which the transformation angle of the wheel rim is 50°. The whole transformation process can be completed in less than 1 s.

In Figure 15(c), the prototype easily overcomes the step as calculated before. Both the RSC wheel and the passive assistant wheel have the shape of three legs in the prototype. Figure 16(a) illustrates the maximum height of the obstacle that the passive assistant wheel can climb, which is $H_m = \sqrt{3l^2 - r^2}$. Here, $l = 9$ cm, $r = 4$ cm and $H_m = 15.07$ cm. The equivalent radius of the passive assistant wheel is $R_e = l + r = 13$ cm, so the obstacle-crossing ability can be evaluated by $H_m/R_e = 1.16$. This value is 1.52 for the RSC wheel and 0.5 for the round wheel as shown in Figure 16(b), which proves that the RSC wheel possesses a better obstacle-crossing performance.

Figure 15(c) also records the centroid trajectory of the robot (approximately considered to be concentrated at the center of the RSC wheel) during the step-climbing process. As shown in Figure 17, taking the initial wheel center position as the origin, the height variation range of the centroid is always within 15 cm and the maximum absolute value of the track slope is 1.0079 in the whole process. Similar to the kinematic analysis in Section 2, before $T = 3$ s, that is, the RSC wheel completely climbs the obstacle, and the trajectory slope is always positive.

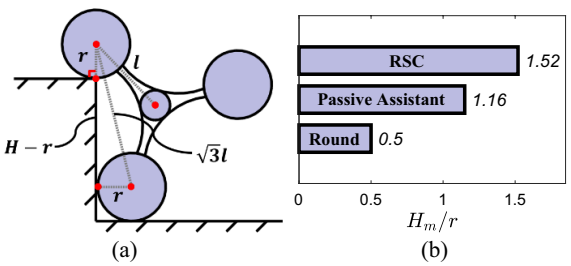

Figure 16 The comparison of the step-climbing capacity: (**a**) The step with maximum height that the passive assistant can climb, (**b**) The H_m/r value of the rim shape changeable (RSC) wheel, the passive assistant wheel and the round wheel

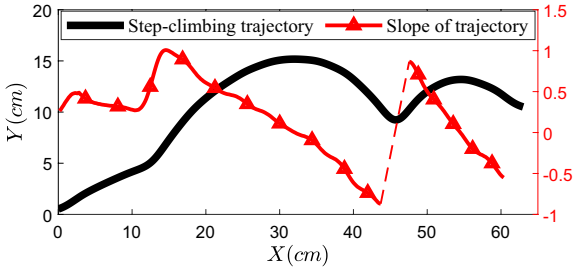

Figure 17 Obstacle-crossing trajectory and the change of slope

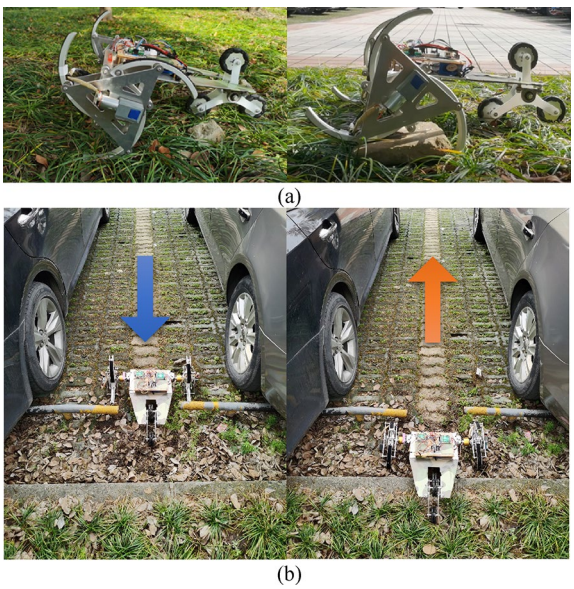

Figure 18 Experiment of traversing different terrains: (**a**) The robot traverses on rough terrain, (**b**) The robot passes through the narrow space in both directions without turning

The fluctuation of the centroid is slight, which proves that the robot has good stability during the obstacle-crossing process.

In addition, as shown in Figure 18, the rough surface locomotion ability and the bi-directional obstacle-crossing performance of the prototype are also examined. It is shown in Figure 18(a) that the prototype can smoothly pass through rough terrain with complex features such as stones and pits, and has strong terrain adaptability. In Figure 18(b), the arrows indicate the direction of motion of the robot. In the narrow space between two cars, it is difficult for the robot to turn around. However, the RSC wheel can transform into forward or backward direction motion mode, allowing the mobile platform to pass through the narrow space in both directions without turning.

6 Conclusions

This work proposes a novel wheel-legged robot with RSC wheels that can switch between wheel mode and leg mode based on a four-bar mechanism. The main contributions are as follows:

(1) A novel transformable mechanism, enabling the robot to maintain both high mobility in flat ground and bi-directional obstacle-crossing performance in rough roads.
(2) A design process that gets rid of the coupling between the geometric structure and the transformation driving mechanism. Based on that, the geometric parameters of the RSC wheel and the design variables of the driving four-bar mechanism are optimized separately to enhance the obstacle-crossing performance and reduce the difficulty of transformation.
(3) A robot with good mobile performance. Experiments show that the prototype equipped with the new wheel mechanism can overcome obstacles with a maximum height of 1.52 times its wheel radius, and run smoothly in rough terrains.

In future research, the passive assistant wheel will be substituted with the active RSC wheel to achieve better bi-directional obstacle-crossing ability. In addition, a vision module will be added to identify the height of obstacles. The rim of the wheel will be transformed into different angles to adapt to different terrains, which can reduce the energy consumption of the robot when performing missions. At the same time, the robot can determine whether the obstacle-crossing is completed based on visual information, thereby switching back from the leg mode to the wheel mode timely to avoid centroid fluctuations in the leg mode shown in Figure 1 where the X coordinate is about 42 cm.

The design process and the transformable mechanism proposed in this paper can provide a reference for the design of the wheel-legged robot. The stable and efficient obstacle-crossing performance of the mobile platform will expand its application in fields such as detection and rescue, and improve the success rate of the missions in complex terrains.

Acknowledgements
Not applicable.

Authors' Contributions
ZF took on most of the research work, including the theoretical research and modeling, prototype experiments and paper writing of the manuscript; HX assisted with the theory researching and method validity; YL assisted with the experiments. WG put forward a great variety of valuable suggestions on some key theory points, so that the research work can be carried out smoothly. All authors read and approved the final manuscript.

Authors' Information
Ze Fu, born in 1999, is currently a master candidate at *State Key Laboratory of Mechanical System and Vibration, Shanghai Jiao Tong University, China*. He received his bachelor's degree from *Xi'an Jiao Tong University, China*, in 2021. His research interests include legged robot and intelligent robotics.
Hao Xu, born in 1998, is currently a master candidate at *State Key Laboratory of Mechanical System and Vibration, Shanghai Jiao Tong University, China*.
Yinghui Li, born in 1999, is currently a PhD candidate at *State Key Laboratory of Mechanical System and Vibration, Shanghai Jiao Tong University, China*.
Weizhong Guo, is currently a professor at *School of Mechanical Engineering, Shanghai Jiao Tong University, China*. He received his PhD degree from *Shanghai Jiao Tong University, China*, in 1999. His research mainly focuses on parallel robots and modern mechanisms.

Funding
Supported by State Key Lab of Mechanical System and Vibration Project of China (Grant No. MSVZD202008).

Data availability
The data that support the findings of this work are available on request from the author, ZF, upon reasonable request.

Declarations

Ethics approval and consent to participate
Not applicable.

Consent for publication
Not applicable.

Competing interests
The authors declare no competing financial interests.

Received: 25 September 2022 Revised: 2 November 2023 Accepted: 6 November 2023
Published online: 18 December 2023

References

[1] Y Kim, Y Lee, S Lee, et al. STEP: A new mobile platform with 2-DOF transformable wheels for service robots. *IEEE-ASME Transactions on Mechatronics*, 2020, 25(4): 1859-1868.
[2] V Larin. Navigation of the wheeled transport robot under measurement noise. *TWMS Journal of Pure and Applied Mathematics*, 2016, 7(1): 20-27.
[3] L Ran, Y Zhang, T Yang, et al. Autonomous wheeled robot navigation with uncalibrated spherical images. *Chinese Conference on Intelligent Visual Surveillance*, 2016: 47-55.
[4] P Nazemzadeh, F Moro, D Fontanelli, et al. Indoor positioning of a robotic walking assistant for large public environments. *IEEE Transactions on Instrumentation and Measurement*, 2015, 64(11): 2965-2976.
[5] J Fabian, G M Clayton. Error analysis for visual odometry on indoor, wheeled mobile robots with 3-D sensors. *IEEE/ASME Transactions on Mechatronics*, 2014, 19(6): 1896-1906
[6] B Ghotbi, F González, J Kövecses, et al. Effect of redundant actuation on the mobility of wheeled robots on unstructured terrain. *2015 ASME International Design Engineering Technical Conferences and Computers and Information in Engineering Conference*, Boston, Massachusetts, USA, 2-5 Aug., 2015: V003T01A016.
[7] R Siegwart, P Lamon, T Estier, et al. Innovative design for wheeled locomotion in rough terrain. *Robotics and Autonomous Systems*, 2002, 40(2-3): 151-162
[8] H Zhang, Y Liu, J Zhao, et al. Development of a bionic hexapod robot for walking on unstructured terrain. *Journal of Bionic Engineering*, 2014, 11(2): 176-187.
[9] C D Remy. Ambiguous collision outcomes and sliding with infinite friction in models of legged systems. *International Journal of Robotics Research*, 2017, 36(12): 1252-1267.
[10] P B Wieber, R Tedrake, S Kuindersma. Modeling and control of legged robots. In: *Handbook of Robotics*,Springer, 2016: 1203–1234.
[11] T Matsuzawa, A Koizumi, K Hashimoto, et al. Crawling motion and foot trajectory modification control for legged robot on rough terrain. *2017 IEEE International Conference on Mechatronics and Automation (ICMA)*, Takamatsu, Japan, 6-9 Aug., 2017: 1976-1982.
[12] K A Daltorio, T E Wei, G D Wile, et al. Mini-Whegs (TM) climbing steep surfaces with insect-inspired attachment mechanisms. *The International Journal of Robotics Research*, 2007, 28(2): 285-302.
[13] U Saranli, M Buehler, D E Koditschek. RHex: A simple and highly mobile hexapod robot. *The International Journal of Robotics Research*, 2001, 20(7): 616-631.
[14] Kwak B, Bae J. Design and analysis of a rotational leg-type miniature robot with an actuated middle joint and a tail (RoMiRAMT), *2015 IEEE/RSJ International Conference on Intelligent Robots and Systems (IROS)*, Hamburg, Germany, 28 Sept.-2 Oct., 2015: 2148-2153.
[15] J Muller, M Schneider, M Hiller. Modeling, simulation, and model-based control of the walking machine ALDURO. *IEEE/ASME Transactions on Mechatronics*, 2000, 5(2), 142-152.
[16] J A Smith, I Sharf, M Trentini. PAW: a hybrid wheeled-leg robot. *Proceedings 2006 IEEE International Conference on Robotics and Automation*, Orlando, FL, USA, 15-19 May, 2006: 4043-4048.
[17] C Grand, F Benamar, F Plumet, et al. Decoupled control of posture and trajectory of the hybrid wheel-legged robot Hylos. *IEEE International Conference on Robotics and Automation,* New Orleans, LA, USA, 26 April-1 May, 2004: 5111–5116.
[18] T Sun, X Xiang, W Su, et al. A transformable wheel-legged mobile robot: Design, analysis and experiment. *Robotics and Autonomous Systems*, 2017, 98: 30-41.
[19] Y Shen, G Zhang, Y Tian, et al. Development of a wheel-paddle integrated quadruped robot for rough terrain and its verification on hybrid mode. *IEEE Robotics and Automation Letters*, 2018, 3(4): 4062–4067.
[20] J B Jeans, D Hong. IMPASS: Intelligent mobility platform with active spoke system. *2009 IEEE International Conference on Robotics and Automation*, IEEE, 2009: 1605–1606.
[21] S C Chen, K J Huang, W H Chen, et al. Quattroped: A leg--wheel transformable robot. *IEEE/ASME Transactions OnMechatronics*, 2014, 19(2): 730–742.
[22] D Y Lee, J K Kim, C Y Sohn, et al. High–load capacity origami transformable wheel. *Science Robotics*, 2021, 6(53): eabe0201.
[23] A Yeldan, A Arora, G S Soh. Quadrunner: A transformable quasi-wheel quadruped. *2022 International Conference on Robotics and Automation (ICRA)*, IEEE, 2022: 4694–4700.
[24] C Zheng, K Lee. WheeLeR: Wheel-leg reconfigurable mechanism with passive gears for mobile robot applications. *2019 International Conference on Robotics and Automation (ICRA)*, Montreal, QC, Canada, 20-24 May, 2019: 9292-9298.
[25] R Mertyuz, A K Tanyldz, B Taar, et al. FUHAR: A transformable wheel-legged hybrid mobile robot. *Robotics and Autonomous Systems*, 2020: 133.
[26] S Ryu, Y Lee, T W Seo. Shape-morphing wheel design and analysis for step climbing in high speed locomotion. *IEEE Robotics and Automation Letters*, 2020, 5(2): 1977-1982.
[27] K A Daltorio, T E Wei, A D Horchler, et al. Mini-whegs TM climbs steep surfaces using insect-inspired attachment mechanisms. *The International Journal of Robotics Research*, 2009, 28(2): 285-302.
[28] Y Kim, G Jung, H Kim, et al. Wheel transformer: A wheel-leg hybrid robot with passive transformable wheels. *IEEE Transactions on Robotics*, 2017, 30(6):1487-1498.